A Fourier Transform Ion Cyclotron Resonance Study of theTemperature and Isotope Effects on the Kinetics of Low-Pressure Association Reactions of Protonated Dimethyl Ether with Dimethyl Ether

Travis D. Fridgen[†] and Terry B. McMahon*[,‡]

Department of Chemistry, University of Waterloo, Waterloo, Ontario, Canada N2L 3G1

Received: August 29, 2000; In Final Form: November 15, 2000

The temperature dependence of the low-pressure association reaction of dimethyl ether with protonated dimethyl ether has been investigated using Fourier transform ion cyclotron resonance mass spectrometry. The unimolecular dissociation of nascent proton-bound dimers is complicated by two factors: (1) the presence of another unimolecular dissociation route producing trimethyloxonium cation and methanol through a high-energy isomer of the proton-bound dimer and (2) the presence of at least two high-energy isomers of the proton-bound dimer en route to dissociation of the nascent proton-bound dimer. RRKM modeling of the experimental temperature dependence of the unimolecular dissociation of nascent proton-bound dimers strongly suggests that dissociation of the nascent proton-bound dimer proceeds through a high-energy isomer. The possible existence of such species is also shown by ab initio calculations. The original mechanism for the ion/molecule reaction and analysis of radiative association kinetics used in the past was found to be too simple for accurate modeling of the reaction between protonated dimethyl ether and dimethyl ether. A slightly more complicated mechanism is proposed which more accurately accounts for the temperature dependence of the unimolecular dissociation to re-form reactants. As well, three isotopomeric variants of the protonated dimethyl ether/dimethyl ether reaction were examined experimentally and theoretically.

Introduction

A central issue in studies of ionic species has been the identification of kinetically stable structural isomers. Metastable dissociation and collision-induced dissociation (CID) studies of a wide variety of organic cations have led to the proposal of novel stable structural isomers such as distonic ions, ion−dipole complexes, hydrogen-bridged radical cations, and enolic tautomers.[1] Infrared multiphoton dissociation (IRMPD) studies on the acetone enol radical cation[2] show that it isomerizes to the keto before dissociation. Threshold photoelectron−photoion coincidence (TPEPICO) spectroscopy has also shown that the radical cations of species such as methyl acetate[3] and propanol[4] also isomerize prior to dissociation. More recently, infrared spectroscopic evidence for two additional isomers of the dichloromethane radical cation has been provided from electron-bombardment matrix isolation studies.[5] These isomers, one having the structure of a distonic radical cation and the other a complex between CH_2Cl^+ and $Cl^{\bullet}$, are predicted to lie slightly higher in energy than the dichloromethane radical cation and have fairly low barriers to isomerization.[6]

The many different isomers that exist for molecular ions suggest that cluster ions may also have a rich chemistry. Although examples are more scarce, ionic clusters have been observed to exist as structurally distinct isomers. For example, clusters of methylated acetone with acetone and dimethyl ether have been formed in a high-pressure (3−7 Torr) ion source where relative abundances of the monomer and cluster ions yield equilibrium constants at various pressures. The van't Hoff plots show clear breaks from linearity which suggests that two isomers of the cluster exist. The first of these was determined to be a covalently bound isomer existing at low temperature, and the second an electrostatically bound and entropically favored isomer which is formed at higher temperatures.[7] Similar studies by Norrman and McMahon[8] on clustering reactions of *tert*-butyl cations with dimethyl ether, diethyl ether, methanol, ethanol, acetone, and acetonitrile, revealed that two structural isomers coexisted for each of these clusters. Enthalpies and entropies of formation for each of the isomers, one electrostatically bound and the other covalently bound, were also determined. In FTICR studies, high-energy hydrogen-bonded isomers of complexes between CH_3^+ and methanol or acetone were shown to exist from the differences in unimolecular decomposition pathways when formed by reaction of CH_3^+ and methanol or acetone in an ICR cell.[9] As well, competition between dissociation and isomerization has been observed in the unimolecular reactions of proton-bound methanol/acetonitrile dimers.[10] More recently, vibrational predissociation spectroscopy used in conjunction with mass detection of the photofragments showed conclusively that $H^+(CH_3OH)_4H_2O$ clusters exist in at least two distinct isomeric forms, one H_3O^+-centered and one $CH_3OH_2^+$-centered.[11]

Low-pressure ion/molecule association reactions are fundamentally quite interesting as the kinetic data gained from these experiments, when compared to results of kinetic models, may aid in the understanding of the very complex potential energy hypersurface on which the ion/molecule complex resides. Comparisons of experimental and modeled rate constants have been shown to lead to fairly accurate dissociation energies for various ion/molecule complexes.[12−16]

Under low-pressure conditions ($<10^{-6}$ mbar) where collisions are rare, the nascent ion/molecule adduct has the possibility of becoming a stabilized complex by emitting an infrared photon before either dissociating back to reactants or being stabilized

* Author to whom correspondence should be addressed.
[†] E-mail tdfridge@sciborg.uwaterloo.ca.
[‡] E-mail mcmahon@sciborg.uwaterloo.ca.

10.1021/jp0030948 CCC: $20.00
Published on Web 01/23/2001

SCHEME 1

$$A^+ + B \underset{k_b}{\overset{k_f}{\rightleftharpoons}} \left[(AB^+)^*\right] \xrightarrow{k_{ra}} AB^+ + h\nu$$

$$\downarrow \beta k_c[B]$$

$$AB^+$$

collisionally (Scheme 1) where β is an efficiency factor for collisional stabilization.

By applying the steady-state assumption to the concentration of $(AB^+)^*$ an apparent bimolecular rate constant for loss of reactants is given by

$$k_{app} = \frac{k_f(k_{ra} + k_c[\mathrm{B}])}{k_b + k_{ra} + k_c[\mathrm{B}]} \quad (1)$$

By performing a Taylor series expansion about [B] = 0 to first order in [B], it is readily shown that the apparent rate constant for formation of AB^+ is[17]

$$k_{app} = \frac{k_f k_{ra}}{k_b + k_{ra}} + \frac{k_b k_f k_c[\mathrm{B}]}{(k_b + k_{ra})^2} \quad (2)$$

If it is assumed that every collision between A^+ and B results in formation of the nascent $(AB^+)^*$ and that every collision between $(AB^+)^*$ and B results in sufficient stabilization of the complex (i.e., $\beta = 1$, the strong collision assumption) to dramatically slow the rate of unimolecular dissociation, then k_f and k_c can be estimated from the calculated collision rate constants. That k_f can be assumed to be the collision rate for the nascent proton-bound dimer of dimethyl ether was shown by McEwen et al.[18] Their experimental k_f was determined to be 2×10^{-9} cm^3 s^{-1} which is comparable to the calculated 1.74×10^{-9} cm^3 s^{-1}. Smith et al.[19] have concluded that the collisional stabilization efficiency for the nascent CH_3^+/CH_3CN complex was only 14% ($\beta = 0.14$) when CH_3CN was the bath gas. They found that typically 525 cm^{-1} (6.3 kJ mol^{-1}) of energy was removed from the nascent complex in a single collison with the CH_3CN bath gas. The removal of this amount of energy would drastically increase the lifetime of the nascent ion/molecule complex resulting in the further removal of energy on subsequent collisions. In this study two exothermic reaction channels, leading to the loss of C_2H_4 and HCN were observed which accounts for the low collision efficiency.

By monitoring the depletion of A^+ at various pressures of neutral reactant and plotting the apparent rate against pressure, the rate constants for radiative stabilization and unimolecular dissociation of the activated complex can be obtained directly, as was first shown by Kofel and McMahon over a decade ago.[17] Since then, many experimental and theoretical examinations of low-pressure association reactions have been reported. To date, however, temperature dependence studies of only a few systems, including acetone/protonated acetone,[20,21] acetone-d_6/protonated acetone-d_6,[20,21] butanone/protonated butanone,[21] NO^+/3-pentanone,[15,21] and Ag^+/acetone,[12] have been reported. With the exception of the last system, the strong temperature dependence of the intercepts of the apparent rate constants vs pressure have been successfully modeled[14,21] supporting the mechanism in Scheme 1.

One interesting complication to measuring the rates of ion/molecule association reactions arises when the stabilization and decomposition processes of the excited complex are in competition with a side reaction. This has been observed in the NO^+/3-pentanone system[15,22] where the association reaction is in competition with an endothermic charge-transfer channel forming the NO radical and 3-pentanone radical cation which is, in fact, the major reaction channel for NO^+ and 3-pentanone. Earlier, the cyanoacetylene radical cation/cyanoacetylene association was found to compete with two side reactions forming $HC_5N^{+\bullet}$ and HCN or $HC_6N_2^+$ and $H^\bullet$.[23] The side reactions were not emphasized in these reports other than to discern the mechanisms for their formation. In addition, in the first example, when modeling the rate constants, attempts were made to include the second reaction channel.

The dimethyl ether/protonated dimethyl ether association reaction has been studied[24,25] previously and it had been observed that the association reaction competes with the reaction to form trimethyloxonium cation and methanol. The latter reaction accounts for roughly 10% (isotope dependent)[24] of the observed depletion of protonated dimethyl ether at 294 K.

The purpose of this work is to examine the temperature and isotope dependence of the association reaction between protonated dimethyl ether and dimethyl ether, thereby obtaining the effect of temperature and isotopic substitution on the unimolecular dissociation and radiative stabilization reaction channels of the nascent proton-bound dimer. By comparing the experimental dependence of k_b on reactant temperature with values obtained using master equation modeling, in conjuction with ab initio-calculated vibrational frequencies, it is argued that the existence of higher-energy isomers of the proton-bound dimer do not allow for the unambiguous experimental determination of k_b for unimolecular dissociation of the nascent proton-bound dimer. A reassessment of the protonated dimethyl ether/dimethyl ether reaction mechanism was done in order to account for this temperature dependence by theoretical means. Also, the experimental radiative stabilization rate constants, k_{ra}, are compared to experimental values for other systems and those calculated on the basis of ab initio infrared intensities.

Experimental Details

All experiments were carried out with a Bruker CMS 47 FT-ICR mass spectrometer equipped with a 4.7 T magnet and a 6 × 6 cm cylindrical ICR cell. The ICR cell is mated to a home-built high-pressure external ion source which has been described in detail previously.[17,20]

Protonated or deuteronated dimethyl ether (or dimethyl ether-d_6) was formed inside the ICR cell by proton transfer from protonated benzene or deuteronated benzene-d_6 to neutral dimethyl ether (or dimethyl ether-d_6). Protonated benzene was generated in the external high-pressure ion source from roughly 400:100:1 mixtures of $CH_4/N_2/C_6H_6$(or C_6D_6) and was transferred to the ICR cell through a system of electrostatic ion optics. After an appropriate delay time to allow for sufficient proton transfer, all ions except the desired protonated or deuteronated reagent ion were ejected from the ICR cell by standard radio frequency (rf) ejection techniques. A second time delay corresponding to an average 5 collisions per ion ensured thermalization of the ions. For example, at the lowest pressures studied, 7×10^{-9} mbar, a 30 s delay was used which corresponds to an average 6 collisions per ion. After this second delay all ions, except for the desired precursor, were

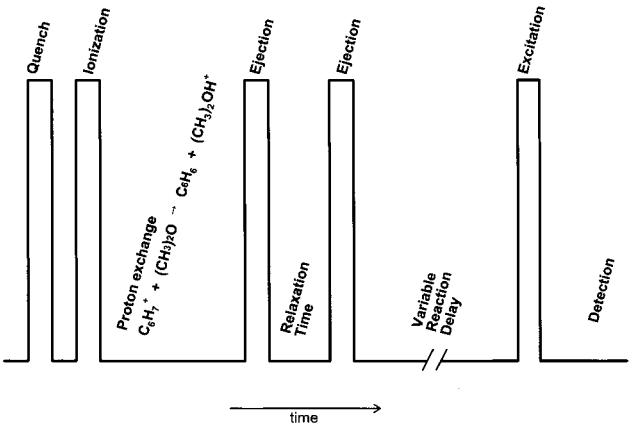

Figure 1. Scan function used for the FT-ICR experiments reported in this work.

once again ejected. The FT-ICR pulse sequence is shown in Figure 1. The neutral dimethyl ether was introduced into the ICR cell via precision leak valves at calibrated pressures from 7×10^{-9} mbar to 1.5×10^{-6} mbar. The pressure gauge was calibrated by observing the kinetics of the following reaction:

$$C_3H_7^+ + (CH_3)_2O \rightarrow C_3H_6 + (CH_3)_2OH^+ \qquad (3)$$

which was assumed to occur at the collision rate. A slower hydride abstraction side reaction producing $CH_3OCH_2^+$ was also observed. The calibration factor for the ion gauge was found to be 1.70 ± 0.06 for dimethyl ether.

Due to stray RF pickup it was impossible to measure the temperature inside the ICR cell during experiments and the temperature inside the ICR cell had to be calibrated. The temperature inside the ICR cell was calibrated to the external temperature of the vacuum housing with iron−constantan thermocouples, one mounted on the vacuum housing and one mounted in contact with the ICR cell. The calibration was constant on two separate occasions before and after the completion of the experiments and was constant over the internal pressure ranges used for these experiments.

The intensities of the desired protonated dimethyl ether, the corresponding proton- or deuteron-bound, dimer and the product of a side reaction, the trimethyl oxonium ion $(CH_3)_3O^+$ were monitored as a function of reaction time up to about 90% conversion of protonated dimethyl ether. Between four and fifty-six transients were accumulated and Gaussian multiplied to enhance the accuracy of the ion abundance measurement. Observed rate constants, k_{obs} for reaction of protonated dimethyl ether were obtained from a least-squares fitting of a semilogarithmic plot of normalized protonated dimethyl ether intensity vs time. The apparent rate constants for the association reactions forming the proton- or deuteron-bound dimers (eqs 4−7)

$$(CH_3)_2OH^+ + (CH_3)_2O \rightarrow [(CH_3)_2O]_2H^+ \qquad (4)$$

$$(CH_3)_2OD^+ + (CH_3)_2O \rightarrow [(CH_3)_2O]_2D^+ \qquad (5)$$

$$(CD_3)_2OH^+ + (CD_3)_2O \rightarrow [(CD_3)_2O]_2H^+ \qquad (6)$$

$$(CD_3)_2OD^+ + (CD_3)_2O \rightarrow [(CD_3)_2O]_2D^+ \qquad (7)$$

were obtained from k_{obs} by using the multiplicative correction factor shown in eq 8 to account for the side reaction producing $(CH_3)_3O^+$,

$$k_{app} = k_{obs} \times \frac{I_{[(CH_3)_2O]_2H^+}}{I_{[(CH_3)_2O]_2H^+} + I_{(CH_3)_3O^+)}} \qquad (8)$$

where I represents the ion intensities of the indicated products. The abundance ratios at all times except $t = 0$ were averaged for use in eq 8. The kinetics of trimethyloxonium cation formation are discussed thoroughly elsewhere.[24] The signal-to-noise ratio at the beginning of each reaction was typically >100. FT-ICR mass spectra of the $(CH_3)_2OH^+/(CH_3)_2O$ association reaction (eq 4) after reaction times of 25 s (i) and 300 s (ii) at a pressure of 1.2×10^{-7} mbar are shown in Figure 2 a. The corresponding semilogarithmic plot of ion intensity vs time is shown in Figure 2 b.

Computational Methods

Ab inito structures, energies, vibrational frequencies, and intensities were all calculated using the B3LYP/6-311G** level of theory and basis set. Calculations were performed using the Gaussian 94[26] computational package. The vibrational frequencies were scaled by a factor of 0.95.[27]

The dipole-corrected ion/polar molecule rate constants, k_f and k_c, were calculated using the trajectory algorithm of Su and Chesnavich.[28] The rate constant for radiative stabilization, k_{ra}, was modeled by standard methods[29] using eq 9[14]

$$k_{ra} = \sum_{i=1}^{N_m} \sum_{n=0}^{\infty} 1.25 \times 10^{-7} n P_i(n) I_i \nu_i^2 \qquad (9)$$

Here, the first summation is over the number of normal modes N_m and the second summation is over the number of levels included, which for practical purposes was about 200, above which there was no change in the calculated rate constant. The ab initio calculated vibrational wavenumbers ν (in cm^{-1}) and intensities I (in km mol^{-1}) were used since, to date, experimental vibrational wavenumbers and intensities for ions are scarce. The canonical distribution of states, $P_i(n)$, was calculated according to eq 10

$$P_i(n,T) = \exp\left(-\frac{h\nu_i n}{k_B T}\right)\left[1 - \exp\left(-\frac{h\nu_i}{k_B T}\right)\right] \qquad (10)$$

where h and k_B are the Planck and Boltzmann constants, respectivily, ν are the vibrational frequencies in s^{-1}, and T is the internal temperature of the newly formed dimer calculated by solving the following equation numerically for T:

$$E_t = \sum_i \left[\frac{h\nu_i N_A}{e^{h\nu_i/k_B T} - 1}\right] \qquad (11)$$

where E_t is the threshold dissociation energy. Average thermal energies of the ion and neutral were used to determine E_t at the various cell temperatures used. Since the dissociation energy (128 kJ mol^{-1})[30] for the proton-bound dimer of dimethyl ether is quite high, T is dominated by the internal temperature and as expected did not display a large ambient temperature dependence.

Theoretical unimolecular dissociation rate constants were obtained from master equation modeling using the VARIFLEX program[31] which uses variational transition state theory (VTST) in order to minimize the RRKM unimolecular dissociation rate

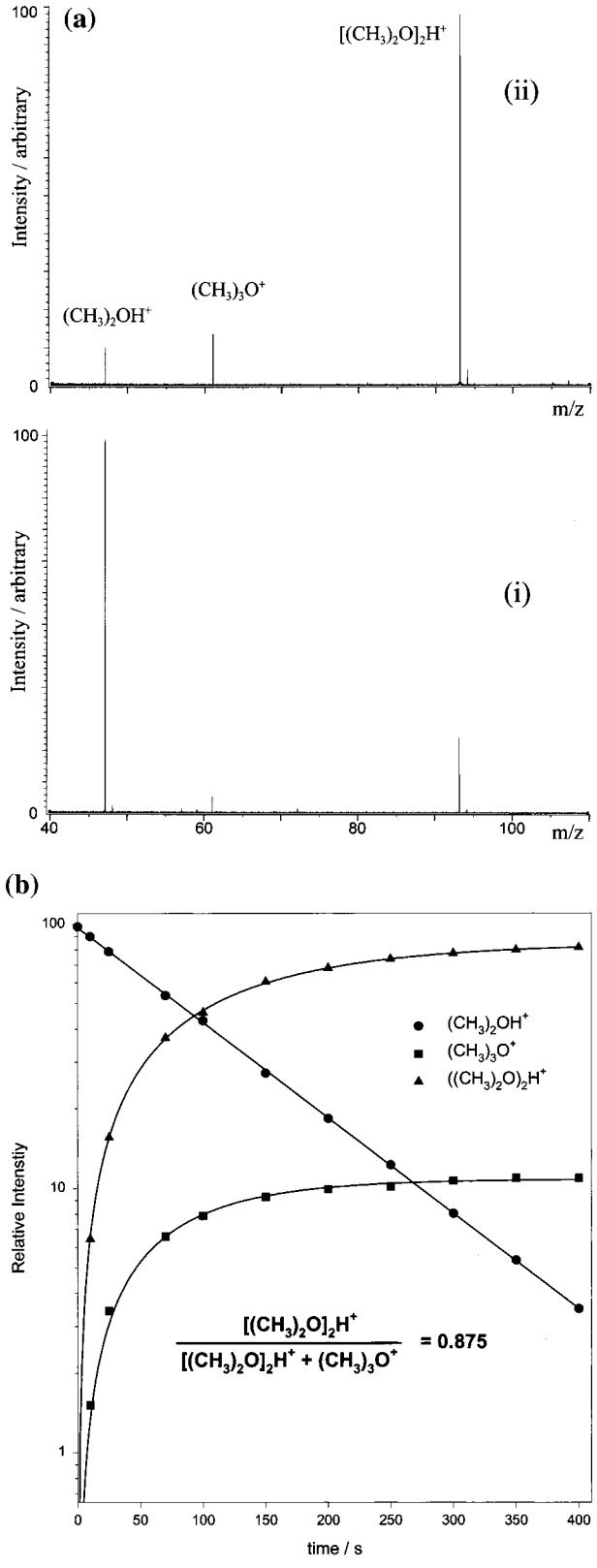

Figure 2. (a) FT-ICR mass spectra obtained for the $(CH_3)_2OH^+$ association reaction at a neutral dimethyl ether pressure of 1.2×10^{-7} mbar and 294 K at reaction times of 25 s (i) and 300 s (ii). (b) Semilogarithmic plot of ion intensity vs reaction time corresponding to the experiment at 1.2×10^{-7} mbar dimethyl ether and 294 K.

constant due to the absence of a well-defined transition state structure for dissociation. B3LYP/6-311G** calculated geometries, vibrational wavenumbers, and intensities were utilized for these calculations.

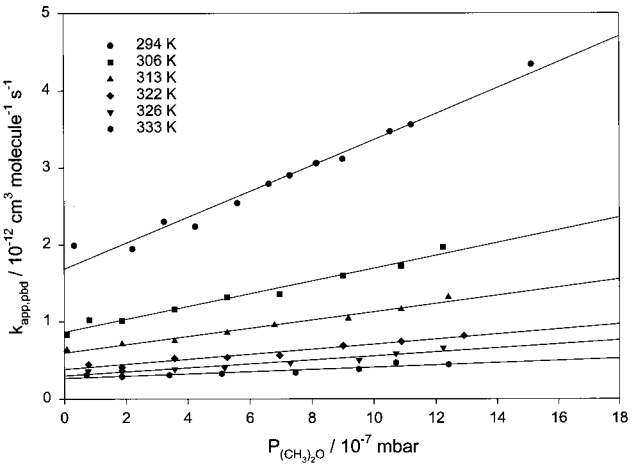

Figure 3. Plot of the apparent rate constant for the formation of the proton-bound dimer of dimethyl ether vs pressure of neutral dimethyl ether at various temperatures.

Results and Discussion

Temperature Dependence. The resultant plots of k_{app} vs pressure of neutral reactant at various ICR cell temperatures are shown in Figure 3. The slopes, intercepts, calculated collision rate constants, as well as experimental rate constants and lifetimes for unimolecular dissociation and radiative stabilization are summarized in Table 1. The temperature dependence on the unimolecular dissociation rate and radiative association rate will now be discussed in turn.

Unimolecular Dissociation. The 313 K experimental unimolecular dissociation rate k_b is 11.1×10^4 s^{-1} while Fisher and McMahon's[25,32] reported 313 K value of 4.1×10^4 s^{-1}, is notably smaller. The earlier measurements by Fisher and McMahon is considered to be in error due to heating of the cell by the internal ionization filament. For the present work, there was no internal ionization and therefore the type of uncertainty in the temperature experienced by Fisher and McMahon was not present in this work. The rate constants reported here are thus deemed to be more reliable.

The unimolecular dissociation rate constant of nascent proton-bound dimethyl ether dimer is expected to increase with temperature due to a larger increase in the sum of states in the transition state compared to the increase in the density of states in the reacting complex. Experimentally, it is seen that this value increases approximately an order of magnitude over the temperature range from 294 to 333 K. The experimental temperature dependence is plotted in Figure 4 (open circles with maxima and minima in the error bars connected with a solid line) along with the values of k_b calculated using VTST for dissociation of the nascent proton-bound dimer of dimethyl ether, the latter denoted by the dashed line and diamonds. It is readily apparent that the functional form of the observed temperature dependence does not resemble at all the VTST-calculated form.

In our attempts to find a transition state separating the proton-bound dimer from dimethyl ether and protonated dimethyl ether, two isomers of the dimer were revealed. By stretching and freezing the bond distance between one of the dimethyl ether oxygen atoms and the binding proton the structure collapsed to one resembling I1 in Figure 5. Further stretching of this bond resulted in a structure resembling IT in Figure 5. The results of this exercise suggest that the dissociation of the proton-bound dimer of dimethyl ether proceeds through the higher energy isomer I1 and finally IT.

The mechanism for reaction of protonated dimethyl ether and dimethyl ether must be somewhat more complicated than is

TABLE 1: Summary of Rate Constants for the Association Reaction between Dimethyl Ether and Protonated Dimethyl Ether at Various Temperatures

	294 K[b]	306 K	313 K	322 K	326 K	333 K
slope/10^{-23} cm^6 s^{-2}	6.81 ± 0.42	3.53 ± 0.20	2.30 ± 0.14	1.45 ± 0.11	1.16 ± 0.11	0.66 ± 0.10
intercept/10^{-13} cm^3 s^{-1}	16.8 ± 1.2	8.65 ± 0.61	5.94 ± 0.36	3.82 ± 0.29	3.00 ± 0.31	2.67 ± 0.24
k_f/10^{-9} cm^3 s^{-1} (calc)[a]	1.75	1.73	1.71	1.70	1.69	1.68
k_c/10^{-9} cm^3 s^{-1} (calc)[a]	1.52	1.50	1.49	1.48	1.47	1.46
k_{uni}/10^4 s^{-1}	3.90 ± 0.41	7.36 ± 0.93	11.1 ± 1.4	17.4 ± 3.0	21.4 ± 4.9	36.8 ± 8.7
k_{ra}/s^{-1}	37.5 ± 5.4	36.8 ± 5.8	38.5 ± 5.8	39.0 ± 8.0	38.0 ± 10.5	58.5 ± 13.9
k_{ra} (calc)/s^{-1}	140	142	143	145	145	146
τ_{uni}/10^{-6} s	25.6 ± 2.9	13.6 ± 1.5	9.0 ± 1.0	5.7 ± 0.7	4.7 ± 0.7	2.7 ± 1.1
τ_{ra}/10^{-2} s	2.67 ± 0.38	2.72 ± 0.40	2.60 ± 0.40	2.56 ± 0.22	2.63 ± 0.60	1.71 ± 0.51
correlation (r)[c]	0.988	0.987	0.988	0.978	0.962	0.940

[a] Dipole-corrected ion−neutral collision rates. [b] Reported also in Table 2. [c] Least-squares fit of the slope and intercept.

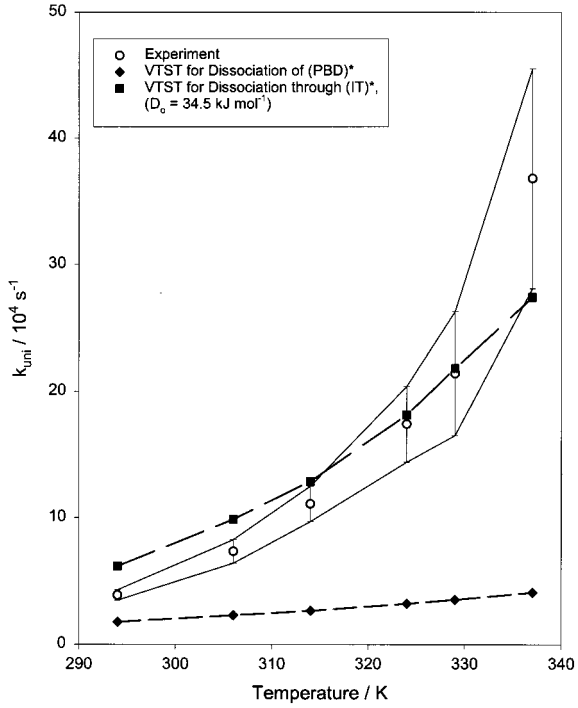

Figure 4. Plot of the experimental and calculated unimolecular dissociation rate constants, k_{uni}, versus temperature. The lines connecting the modeled rate constants are simply to guide one's eye. The thin solid lines connect the maxima and minima of the experimental rate constants.

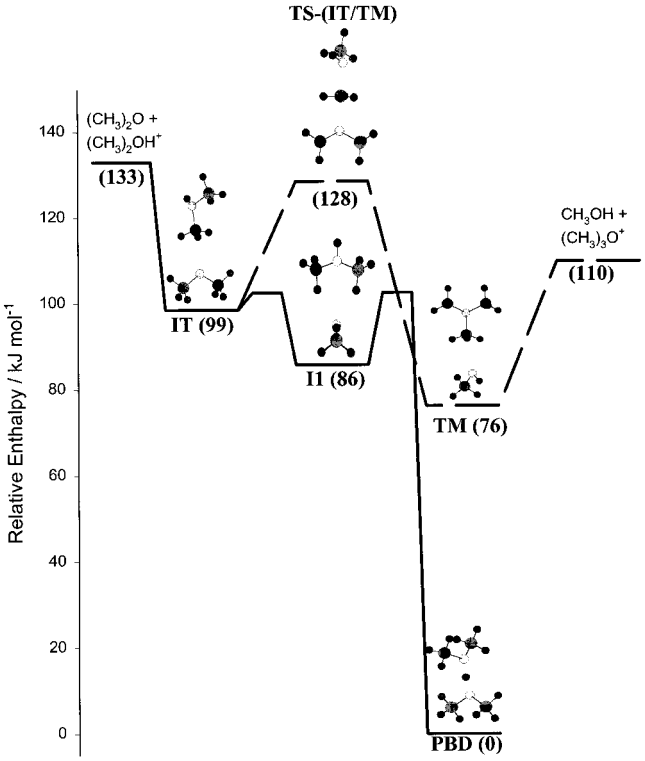

Figure 5. B3LYP/6-311G** calculated energy diagram for the protonated dimethyl ether dimer.

given in Scheme 1. The proposed mechanism including IT dissociating to trimethyloxonium cation is shown in Scheme 2 where (PBD)* is the nascent proton-bound dimer of dimethyl ether and (IT)* and (I1)* are the isomers of the nascent proton-bound dimer of dimethyl ether en route to dissociation (see Figure 5). The species (IT)* isomerizes to (I1)* which isomerizes to PBD*, with rate constants k_{t1} and k_{1p} and isomerization rate constants for the reverse reactions k_{1t} and k_{p1}, respectively.

The species, (IT)* can also dissociate to form trimethyloxonium cation and methanol with a rate constant k_t. A steady-state analysis on each of the nascent isomers yields the following expression for the apparent rate constant for formation of proton-bound dimer $k_{app,pbd}$,

$$k_{app,pbd} = \{k_f(k_c[(CH_3)_2O] + k_{ra})(k_{t1}k_{1p})\}/\{[k_{1t}(k_{ra} + k_c[(CH_3)_2O] + k_{p1}) + k_{1p}(k_{ra} + k_c[(CH_3)_2O])](k_t + k_b) + k_{t1}k_{1p}(k_{ra} + k_c[(CH_3)_2O])\} \quad (12)$$

Since k_{ra} and $k_c[(CH_3)_2O]$ are small, the first term in the denominator reduces to $k_{1t} \times k_{p1}$. Similarly, since k_b is presumably substantially larger than k_t due the large entropic barrier associated with dissociation of (IT)* to trimethyloxonium cation and methanol eq 12 can be rewritten,

$$k_{app,pbd} = \{k_f(k_c[(CH_3)_2O] + k_{ra})(k_{t1}k_{1p})\}/\{[k_{1t}k_{p1} + k_{1p}(k_{ra} + k_c[(CH_3)_2O])]k_b + k_{t1}k_{1p}(k_{ra} + k_c[(CH_3)_2O])\} \quad (13)$$

The second term within the square brackets in the denominator of eq 13 is small compared to the product of the two isomerization rate constants which are comparably fast. Elimination of this term from eq 13 yields

$$k_{app,pbd} = \frac{k_f(k_c[(CH_3)_2O] + k_{ra})(k_{t1}k_{1p})}{k_{1t}k_{p1}k_b + k_{t1}k_{1p}(k_{ra} + k_c[(CH_3)_2O])} \quad (14)$$

Division through eq 14 by $k_{t1} \times k_{1p}$ produces

$$k_{app,pbd} = \frac{k_f(k_c[(CH_3)_2O] + k_{ra})}{\frac{k_{1t}}{k_{t1}}\frac{k_{p1}}{k_{1p}}k_b + k_{ra} + k_c[(CH_3)_2O]} \quad (15)$$

SCHEME 2

$$(CH_3)_2OH^+ + (CH_3)_2O \xrightarrow{k_f} (IT)^* \xrightarrow{k_b} (CH_3)_2OH^+ + (CH_3)_2O$$

$$(IT)^* \xrightarrow{k_t} (CH_3)_3O^+ + CH_3OH$$

$$(IT)^* \underset{k_{1t}}{\overset{k_{t1}}{\rightleftharpoons}} (I1)^* \underset{k_{p1}}{\overset{k_{1p}}{\rightleftharpoons}} (PBD)^* \xrightarrow{k_{ra}} [(CH_3)_2O]_2H^+ + h\nu$$

$$(IT)^* \xrightarrow{k_c[(CH_3)_2O]} [(CH_3)_2O]_2H^+$$

which, upon performing a Taylor series expansion about $[(CH_3)_2O] = 0$ and making the assumption that k_{ra} is small compared to the term containing k_b, yields

$$k_{app,pbd} = \frac{k_f k_{ra}}{\frac{k_{1t}}{k_{t1}}\frac{k_{p1}}{k_{1p}}k_b} + \frac{k_f k_c[(CH_3)_2O]}{\frac{k_{1t}}{k_{t1}}\frac{k_{p1}}{k_{1p}}k_b} \tag{16}$$

Qualitatively, eqs 2 and 16 are quite similar. The difference is that the slope of the $k_{app,pbd}$ vs pressure plot for the mechanism in Scheme 2 yields the unimolecular dissociation rate constant for isomer (IT)* weighted by what are effectively equilibrium constants governing the relative concentrations of (PBD)*, (IT)*, and (I1)*. This product is abbreviated k_{uni}:

$$k_{uni} = \frac{k_{1t}}{k_{t1}}\frac{k_{p1}}{k_{1p}}k_b \tag{17}$$

Assuming that the transition states for isomerization of the nascent dimers are the same as for the reverse isomerization reactions, the two ratios of isomerization rate constants in eq 15 can be written in terms of simple RRKM theory as

$$\frac{k_{1t}}{k_{t1}}\frac{k_{p1}}{k_{1p}} = \frac{\frac{\sigma}{h}\frac{N^{\ddagger}(I1 \rightarrow IT)}{\rho(I1)}\frac{\sigma}{h}\frac{N^{\ddagger}(PBD \rightarrow I1)}{\rho(PBD)}}{\frac{\sigma}{h}\frac{N^{\ddagger}(I1 \rightarrow IT)}{\rho(IT)}\frac{\sigma}{h}\frac{N^{\ddagger}(PBD \rightarrow I1)}{\rho(I1)}} \tag{18}$$

where the $N^{\ddagger}$ are sums of states from E_0 to E for the transition states specified in brackets, the ρ are densities of states at energy E for the species specified in brackets, and σ and h are the symmetry numbers and Planck's constant, respectively. After cancellations eq 18 reduces to

$$\frac{k_{1t}}{k_{t1}}\frac{k_{p1}}{k_{1p}} = \frac{\rho(IT)}{\rho(PBD)} \tag{19}$$

Substitution of eq 19 into eq 15 yields an expression for k_{uni}

$$k_{uni} = \frac{\rho(IT)}{\rho(PBD)}k_b \tag{20}$$

which can be used to make theoretical estimates of k_{uni} to compare with experiment.

The densities of states can be calculated for the isomeric protonated dimers IT and PBD using the direct count algorithm of Beyer and Swinehart[33] and the rate constant for dissociation of (IT)* to reactants is calculated using VARIFLEX as described above. The plot in Figure 4 denoted by the squares and dashed lines is the modeled value using a dissociation energy of 34.5 kJ mol^{-1}, which is the dissociation energy calculated by ab initio methods. It is clear that the functional form of the temperature dependence of k_{uni} is much better, and the agreement with the experimental values is much better, in many cases within the reported experimental error. It should be noted that the calculated dissociation energy does not take into account basis set superposition error. Utilizing a lower dissociation energy does not affect greatly the outcome of the calculations. A lower dissociation energy significantly increases k_b but also significantly lowers the value of $\rho(IT)/\rho(PBD)$.

It is clear that neglect of dissociation through a higher-energy isomer produces a serious contradiction between theory and experiment. Infrared multiple photon dissociation of proton-bound diethyl ether dimers $(DEE)_2H^+$,[34] perfluoropropylene radical cations,[34] and the proton-bound fluoride−methoxide anion[35] have been studied at low pressure with a pulsed CO_2 laser. Fluence studies of the onset of dissociation showed an induction period, explained as the fluence before the dissociating ion reaches a steady state between photon absorption, emission, and unimolecular decomposition followed by an increase in dissociation with laser fluence. Master equation modeling of the dissociation vs laser fluence curves agree quite well for the species mentioned above except for $(DEE)_2H^+$. For this species the calculated induction period was determined to be significantly larger than that observed experimentally. In other words, the ions are observed to dissociate faster at low laser fluence than predicted by the Master equation modeling. No explanation for this discrepancy was offered. A very plausible explanation for this behavior, though, is that dissociation occurs through a high-energy isomer of the proton-bound dimer, which increases the rate of dissociation in the case of $(DEE)_2H^+$ as determined in this study for the proton-bound dimer of dimethyl ether. The higher-energy $(DEE)_2H^+$ dimers dissociate faster, leading to a lower induction period than is predicted by the Master equation model due to neglect of the higher-energy dimer.

The results of this study are quite interesting since it has been proposed and shown that accurate binding energies of ion/molecule complexes can be obtained by a method similar to that described above using radiative association kinetics and VTST.[14] The best estimate of the 0 K binding energy of the acetone/protonated acetone complex by this method was 130 kJ mol^{-1} in good agreement with with the accepted value. As shown in this study, the contradiction between experiment and theory would be expected to be more pronounced in a

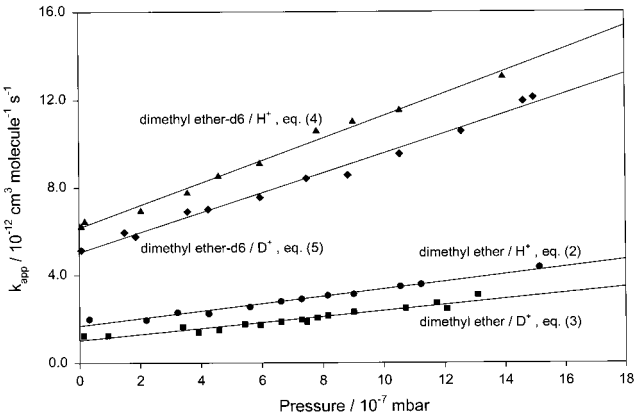

Figure 6. Plot of apparent rate constants vs pressure of neutral dimethyl ether (or -d_6) for reactions 2−5 at 294 K.

temperature-dependence study. Klippenstein et al.[14] modeled the 300.7 and 320.2 K slopes and intercepts of the protonated acetone/acetone reaction. An analysis of their calculated values produces 3.2×10^4 and 4.7×10^4 s^{-1}, respectively, for k_b which are in good agreement with experimental values[20] (2.4×10^4 and 4.7×10^4 s^{-1} respectively), although it should be noted that the experimental temperature dependence is not quite reproduced. The other known isomers for the proton-bound dimer of acetone[36] are a covalently bound structure, where the oxygen of acetone is bound to the carbonyl carbon of protonated acetone, and an enol dimer. The formations of these isomers very likely have a significant barrier for their formation from acetone and protonated acetone making the proton-bound dimer the only important species in the entrance channel to formation and, therefore, the exit channel to dissociation. It should be noted though that the method proposed by Klippenstein et al.[14] of obtaining binding energies does provide good estimates. According to this discussion, the values are a lower limit to the true binding energy, especially for organic complexes which may dissociate through a higher-energy isomer. This type of analysis, however, is expected to be quite good for species which are not expected to have isomeric structures such as atom−organic cation complexes.[12,15]

Radiative Association. Within the experimental uncertainty no real temperature dependence is seen in the rate constant for radiative association. The internal temperature of the (PBD)* ions is estimated to be 840 K at 294 K and increases to 858 K at 333 K, resulting in a calculated radiative association rate constant increasing from 140 s^{-1} at 294 K to 146 s^{-1} at 333 K (see Table 1). There is obviously a large discrepancy, between the magnitudes of the theoretical and experimental k_{ra}. The dependence of k_{ra} on the vibrational wavenumbers comes from calculation of the internal temperature using eq 11 and the ν^2 term in eq 9. The calculated value of k_{ra} is also strongly dependent upon ab initio calculated infrared intensities for which there is no known scaling factor due to the lack of experimental values with which to compare. To bring the k_{ra} value of 140 down to agree with experiment a scaling factor of 0.27 for the calculated intensities is required. It is worth noting that using wavenumbers and intensities calculated at the MP2/6-31G** (wavenumbers scaled by the suggested 0.937[27]) the calculated k_{ra} is 150 s^{-1}, very close to the B3LYP/6-311G** value. Experimentally derived k_{ra} values for nascent proton-bound acetone dimer are 102 and 103 s^{-1} at room temperature.[20,21] By the same method that is used here, Ryzhov et al.[21] calculate k_{ra} to be somewhat higher at 170 s^{-1}. Disagreements of this magnitude between experimental values of k_{ra} and theoretical values derived using calculated infrared intensities are not uncommon.[37] One possible problem with the method of calculation is that we are using vibrational wavenumbers and intensities which are expected to be characteristic of those for the $0 \leftarrow 1$ vibrational transition. At the internal energies of the species radiating (some 126 kJ mol^{-1}) the anharmonicity would act to reduce the magnitude of the vibrational wavenumbers. The lower vibrational frequencies would affect the calculation of k_{ra} by the ν^2 term and that the internal temperature would be lower. Furthermore, the intensities of the emission from these modes would be drastically reduced resulting in a further lowering of the calculated emission rate.

Note that emission of an infrared photon from one of the higher energy isomers is not considered. This is not likely a source of error between the experimental and calculated values as the ratio of (IT)*/(PBD)* is expected to be very small. Furthermore, the lifetime of (IT)* or any isomer with such a small dissociation energy would be so short that slow photon emission is not at all competitive. For systems with isomeric structures that have similar energies to the most stable isomer, radiative stabilization of the isomers may be an important process.

It is worthwhile to compare the experimental k_{ra} values for the nascent acetone and dimethyl ether complexes. The internal temperature of the acetone proton-bound dimer is expected to be lower than the internal temperature of dimethyl ether proton-bound dimer due to the extra six vibrational modes in the former. This would result in a lower k_{ra} for the acetone proton-bound dimer, however, the experimental results show that the dimethyl ether proton-bound dimer radiates much more slowly. This can be explained since acetone proton-bound dimers have two chromophores, C═O bonds, above 1600 cm^{-1} which are predicted to have significant intensity (above 1000 km mol^{-1})[14] and which are not present in the dimethyl ether proton-bound dimers.

Isotope Effect. In Figure 6 are shown plots of k_{app} vs the pressure of neutral precursor for the four association reactions

TABLE 2: Summary of Rate Data for the Isotope Dependence of Low-Pressure Dimethyl Ether Association Reactions (294 K)

	dimethyl ether H$^{+(b)}$	dimethyl ether D$^+$	dimethyl ether-d_6 H$^+$	dimethyl ether-d_6 D$^+$
slope/10^{-22} cm^6 s^{-2}	0.68 ± 0.04	0.55 ± 0.04	2.07 ± 0.07	1.86 ± 0.07
intercept/10^{-12} cm^3 s^{-1}	1.68 ± 0.12	1.03 ± 0.14	7.16 ± 0.24	5.04 ± 0.26
k_l/10^{-9} cm^3 s^{-1} (calc)[a]	1.75	1.74	1.64	1.64
k_c/10^{-9} cm^3 s^{-1} (calc)[a]	1.52	1.52	1.43	1.43
k_{uni}/10^4 s^{-1}	3.90 ± 0.41	4.8 ± 0.9	1.13 ± 0.07	1.26 ± 0.10
k_{uni}(calc)[c]/10^4 s^{-1}	(6.1)	(4.1)	(0.69)	(0.56)
k_{ra}/s^{-1}	37.5 ± 5.4	28.6 ± 7.7	42.6 ± 3.6	38.8 ± 4.1
k_{ra} (calc eq 9)/s^{-1}	(140)	(79)	(134)	(77)
τ_{uni}/10^{-5} s	2.56 ± 0.29	2.08 ± 0.42	8.85 ± 0.59	7.94 ± 0.65
τ_{ra}/10^{-2} s	2.67 ± 0.38	3.50 ± 1.02	2.34 ± 0.19	2.58 ± 0.27
correlation (r)[d]	0.988	0.963	0.995	0.993

[a] Dipole-corrected ion−neutral collision rates. [b] Also reported in Table 1. [c] Calculated using RRKM and VTST as discussed in the text. [d] Least-squares fit of the slope and intercept.

given by eqs 4 to 7. The experimental rate constants k_{uni} and k_{ra} obtained from both the slope and intercept of these plots, as well as the corresponding lifetimes and calculated collision rates are summarized in Table 2. As above, the unimolecular and radiative association rate constants will be discussed in sequence, respectively.

Unimolecular Dissociation. Comparing the unimolecular dissociation rates of the various isotopomeric reactions studied here and reported in Table 2 with those from the protonated acetone/acetone study[20] it is evident that the same trend is observed. Within the reported experimental uncertainty the rate of unimolecular dissociation for protonated or deuteronated dimethyl ether dimers is the same. This similar agreement is also seen for the dimethyl ether-d_6 dimers. The rate constants for dimethyl ether-d_6 dimers are substantially smaller (by a factor of 3.5) than the dimethyl ether-h_6 dimers which is comparable to the 3-fold decrease for the acetone system. This decrease has been ascribed[20] to the increase in the density of states for the deuterated species due to the lower C−D stretching wavenumbers. It should be noted that the number of states in the transition state should also increase, but that the increase in the density of states in the dissociating ions must be more significant. The unimolecular rate constants calculated in the same manner as discussed above compare favorably in that the correct ordering of the rate constants for the dissociation of the -h_{12} and -d_{12} dimers is reproduced. Theory predicts that k_{uni} should be smaller for the deuteron-bound dimers than the proton-bound dimers which is not experimentally discernible due to the magnitude of the error associated with the experimental values.

Radiative Association. Within the error limits reported in Table 2 there is no substantial isotope effect observed, although k_{ra} for deuteron-bound dimethyl ether dimer does have a substantially smaller value than that of the proton-bound dimer and there is much less of a difference between the proton- and deuteron-bound dimers of dimethyl ether-d_6. Calculations based on eq 9 and ab initio wavenumbers and intensities predict k_{ra} to be substantially higher, which was discussed above with respect to the temperature dependence. Furthermore the calculations predict substantially lower photon emission rate constants for the deuteron-bound dimers. The main modes that are responsible for photon emission are the very intense bands corresponding to motion of the proton (or deuteron) between monomers (asymmetric stretch). The ab initio calculations predict that the proton-bound dimers have two such modes with substantial intensity associated with them. The slightly lower intensity and slightly lower vibrational frequency are responsible for the slight decrease in the calculated k_{ra} for the -d_6 species. The deuteron-bound dimers were predicted to have only one asymmetric stretching mode with a lower frequency of vibration than in the proton-bound dimers which is responsible for the substantially lower calculated (almost half) k_{ra} for the deuteron-bound dimers. Since the theoretical framework of eq 9 has been successful in many cases we attribute the disagreement in calculated k_{ra} to the use of ab initio intensities which seem to predict the substantial loss of intensity for one of the asymmetric stretches in the deuteron-bound dimers or an extra intense asymmetric stretch for the proton-bound dimer. Without experimental values for ion vibrational modes and intensities this disagreement is unresolved.

Conclusions

It is clearly illustrated that for the low-pressure reaction of dimethyl ether with protonated dimethyl ether, the kinetics obtained are much more complicated than the previous mechanism suggests. In particular, it is impossible to obtain unambiguously a unimolecular dissociation rate constant for the elementary dissociation of the nascent proton-bound dimer of dimethyl ether which is lowest-energy isomer on the potential energy hypersurface. It has been proposed that dissociation of the nascent ion/molecule complex proceeds through a high-energy isomer and that the unimolecular dissociation rate constant obtained from these types of experiments is actually that of the higher energy isomer weighted by what is effectively an equilibrium constant governing the relative concentrations of the high-energy isomer and the proton-bound dimer. It is still possible to obtain the rate constant for radiative stabilization of the nascent proton-bound dimer, however, there is disagreement between experimental values and those calculated which is attributed to the ab initio calculated infrared intensities and the neglect of anharmonicity in the frequencies and intensities used to calculate radiative emission rate constants.

Acknowledgment. The financial support of the Research Grants Program of the Natural Sciences and Engineering Research Council of Canada (NSERC) is acknowledged. T.D.F. gratefully acknowledges the Postdoctoral Fellowship granted by NSERC. The authors also acknowledge the helpful discussions with Prof. David M. Wardlaw, Prof. Robert Dunbar, and Prof. Micheal T. Bowers with respect to the kinetic modeling.

References and Notes

(1) Studies have been conducted on very many systems and the examples given here are only a drop in the bucket: (a) Holmes, J. L.; Terlouw, J. K.; Lossing, F. P. *J. Phys. Chem.* **1976**, *80*, 2860. (b) Huntress, W. T., Jr.; Sharma, D. K. S.; Jennings, K. R.; Bowers, M. T. *Int. J. Mass Spectrom. Ion Physics* **1977**, *24*, 25. (c) Burgers, P. C.; Holmes, J. L.; Hop, C. E. C. A.; Terlouw, J. K. *Org. Mass Spectrom.* **1986**, *21*, 549. (d) Schaftenaar, G.; Postma, R.; Ruttink, P. J. A.; Burgers, P. C.; McGibbon, G. A.; Terlouw, J. K. *Int. J. Mass Spectrom. Ion Processes* **1990**, *100*, 521.

(2) Osterheld, T. H.; Brauman, J. I. *J. Am. Chem. Soc.* **1993**, *115*, 10311.

(3) Mazyar, O. A.; Mayer, P. M.; Baer, T. *Int. J. Mass Spectrom. Ion Processes* **1997**, 167/*168*, 389.

(4) Booze, J. A.; Baer, T. *J. Phys. Chem.* **1992**, *96*, 5715.

(5) Fridgen, T. D.; Zhang, X. K.; Parnis, J. M.; March, R. E. *J. Phys. Chem. A* **2000**, *104*, 3487.

(6) Lewars, E. G. *THEOCHEM* **1998**, *425*, 207.

(7) Szulejko, J. E.; McMahon, T. B. *Org. Mass Spectrom.* **1993**, *28*, 1009.

(8) Norrman, K.; McMahon, T. B. *J. Am. Chem. Soc.* **1996**, *118*, 2449.

(9) Audier, H. E.; Koyanagi, G. K.; McMahon, T. B.; Tholmann, D. *J. Phys. Chem.* **1996**, *100*, 8220.

(10) Mayer, P. M. *J. Phys. Chem. A* **1999**, *103*, 3687.

(11) Chaudhuri, C.; Jiang, J. C.; Wang, X.; Lee, Y. T.; Chang, H.-T. *J. Chem Phys.* **2000**, *112*, 7279.

(12) Ho, Y.-P.; Yang, Y.-C.; Klippenstein, S. J.; Dunbar, R. C. *J. Phys. Chem. A* **1997**, *101*, 3338.

(13) Dunbar, R. C.; Klippenstein, S. J.; Hrušák, J.; Stöckigt, D.; Schwartz, H. *J. Am. Chem. Soc.* **1996**, *118*, 5277.

(14) Klippenstein, S. J.; Yang, Y.-C.; Ryzhov, V.; Dunbar, R. C. *J. Chem. Phys.* **1996**, *104*, 4502.

(15) Ryzhov, V.; Klippenstein, S. J.; Dunbar, R. C. *J. Am. Chem. Soc.* **1996**, *118*, 5462.

(16) Lin, Y.; Ridge, D. P.; Munson, B. *Org. Mass Spectrom.* **1991**, *26*, 550.

(17) Kofel, P.; McMahon, T. B. *J. Phys. Chem.* **1988**, *92*, 6174.

(18) McEwan, M. J.; Denison, A. B.; Anicich, V. G.; Huntress, W. T., Jr. *Int. J. Mass Spectrom. Ion Processes* **1987**, *81*, 247.

(19) Smith, S. C.; Wilson, P. F.; Sudkeaw, P.; Maclagan, R. G. A. R.; McEwan, M. J.; Anicich, V. G.; Huntress, W. T. *J. Phys. Chem.* **1993**, *98*, 1944.

(20) Thölmann, D.; McCormick, A.; McMahon, T. B. *J. Phys. Chem.* **1994**, *98*, 1156.

(21) Ryzhov, V.; Yang, Y.-C.; Klippenstein, S. J.; Dunbar, R. C. *J. Phys. Chem. A* **1998**, *102*, 8865.

(22) Weddle, G.; Dunbar, R. C. *Int. J. Mass Spectrom. Ion Processes* **1994**, *134*, 73.

(23) Sen, A. D.; Huntress, W. T., Jr.; Anicich, V. G.; McEwan, M. J.; Denison, A. B. *J. Chem. Phys.* **1991**, *94*, 5462.

(24) Fridgen, T. D.; McMahon, T. B. *J. Am. Chem. Soc.*, submitted.

(25) Fisher, J. J.; McMahon, T. B. *Int. J. Mass Spectrom. Ion Processes* **1990**, *100*, 701.

(26) Frisch, M. J.; Trucks, G. W.; Schlegel, H. B.; Gill, P. M. W.; Johnson, B. G.; Robb, M. A.; Cheeseman, J. R.; Keith, T.; Petersson, G. A.; Montgomery, J. A.; Raghavachari, K.; Al-Laham, M. A.; Zakrzewski, V. G.; Ortiz, J. V.; Foresman, J. B.; Cioslowski, J.; Stefanov, B. B.; Nanayakkara, A.; Challacombe, M.; Peng, C. Y.; Ayala, P. Y.; Chen, W.; Wong, M. W.; Andres, J. L.; Replogle, E. S.; Gomperts, R.; Martin, R. L.; Fox, D. J.; Binkley, J. S.; Defrees, D. J.; Baker, J.; Stewart, J. P.; Head-Gordon, M.; Gonzalez, C.; Pople, J. A. *Gaussian 94*, revision C.3; Gaussian, Inc.: Pittsburgh, PA, 1995.

(27) Scott, A. P.; Radom, L. *J. Phys. Chem.* **1996**, *100*, 16502.

(28) Su, T.; Chesnavich, W. J. *J. Chem. Phys.* **1982**, *76*, 5183.

(29) Shi, J.; Bernfeld, D.; Barker, J. R. *J. Chem. Phys.* **1988**, *88*, 6211.

(30) Average of values from (a) Szulejko, J. **1992** unpublished result of 127 kJ mol^{-1}. (b) Meot-Ner, M.; Sieck, L. W. *J. Am. Chem. Soc.* **1991**, *113*, 4448. (c) Meot-Ner, M. *J. Am. Chem. Soc.* **1984**, *106*, 1257. (d) Grimsrud, E. P.; Kebarle, P. *J. Am. Chem. Soc.* **1973**, *95*, 7939.

(31) Klippenstein, S. J.; Wagner, A. F.; Dunbar, R. C.; Wardlaw, D. M.; Robertson S. H. *VARIFLEX, VERSION 1.00* **1999,** July 16.

(32) Note that there is an error in the value reported by Fisher and McMahon. The calculated k_f is reported there to be 0.9×10^{-9} $cm^3 molecule^{-1}$ s^{-1} whereas it should be roughly 1.7×10^{-9} cm^3 $molecule^{-1}$ s^{-1} which does not change the reported kra significantly, but does change the value of k_b from 2.2×10^4 s^{-1} to 4.1×10^4 s^{-1}.

(33) Beyer, T.; Swinehart, D. R. *ACM Commun.* **1973**, *16*, 379.

(34) Jasinski, J. M.; Rosenfeld, R. N.; Meyer, F. K.; Brauman, J. I. *J. Am. Chem. Soc.* **1982**, *104*, 652.

(35) Rosenfeld, R. N.; Jasinski, J. M.; Brauman, J. I. *J. Am. Chem. Soc.* **1982**, *104*, 658.

(36) McCormick, A. M., M.Sc. Thesis, University of Waterloo, Waterloo, Ontario, Canada, 1996.

(37) Personal communication between T. D. F. and Robert Dunbar, May 16, 2000.